Flux-torque cross-coupling analysis of FOC schemes: Novel perturbation rejection characteristics ☆

Luis Amezquita-Brooks [1,a,*], Eduardo Liceaga-Castro [a,1], Jesús Liceaga-Castro [2,b],
Carlos E. Ugalde-Loo [3,c]

[a] CIIIA-FIME, Universidad Autónoma de Nuevo León, Monterrey, Km 2.3 Carr. a Salinas Victoria, C.P. 66600, Apodaca Nuevo León, México
[b] Depto. de Electrónica UAM-Azcapotzalco, D.F., Avenida San Pablo 180, Azcapotzalco, Reynosa Tamaulipas, 02200 Ciudad de México, D.F., México
[c] School of Engineering, Cardiff University, Queen's Buildings, The Parade, Cardiff, CF24 3AA, Wales, UK

ABSTRACT

Field oriented control (FOC) is one of the most successful control schemes for electrical machines. In this article new properties of FOC schemes for induction motors (IMs) are revealed by studying the cross-coupling of the flux-torque subsystem. Through the use of frequency-based multivariable tools, it is shown that FOC has intrinsic stator currents disturbance rejection properties due to the existence of a *transmission zero* in the flux-torque subsystem. These properties can be exploited in order to select appropriate feedback loop configurations. One of the major drawbacks of FOC schemes is their high sensitivity to slip angular velocity perturbations. These perturbations are related to variations of the rotor time constant, which are known to be problematic for IM control. In this regard, the effect that slip angular velocity perturbations have over the newly found perturbation rejection properties is also studied. In particular, although perturbation rejection is maintained, deviations to the equilibrium point are induced; this introduces difficulties for simultaneous flux and torque control. The existence of equilibrium point issues when flux and torque are simultaneously controlled is documented for the first time in this article.

© 2015 The Authors. Published by Elsevier Ltd. ISA. All rights reserved.

1. Introduction

Induction motors (IMs) are widely used as actuators in many industrial and research applications. Along the last decades the evolution of digital processing systems and power electronics made possible the extended use of high-performance IM control systems such as *field oriented control* (FOC) and *direct torque control* (DTC). Among these control strategies FOC has been shown to be a viable every-day solution for most applications [1,2]. There are many kinds of FOC schemes; however, the most successful are based on rotor flux and torque decoupling [3]. Several recent

schemes proposed in the literature are designed under this strategy [1,4–9], which aims at modifying the behavior of the IM into that of a classical *direct current* (DC) motor. With DC motors it is easy to manipulate the flux and the torque separately by driving different physical currents; namely field and armature currents. To achieve this commodity in IMs, non-linear control elements are introduced in order to have virtual flux and torque producing currents. This strategy is commonly implemented following a two-step procedure [1–3,10]. The first step consists in controlling the stator currents using a *voltage source inverter* (VSI) as an actuator. By controlling the stator currents, the fifth degree non-linear model of the IM may be simplified into a third order system. The second step is to design a non-linear flux-torque control law for this system. It is in this second step that most FOC schemes are introduced. Control strategies other than FOC may be used in the second step while preserving the stator currents control loop; however, they are akin to FOC in this regard [11–15].

After attaining control of the stator currents most IM control strategies aim at decoupling the flux-torque subsystem. However, this system has intrinsic *dynamical* cross-coupling properties which have not been fully studied. Even when typical FOC schemes are fairly disseminated, their coupling characteristics

Symbol		S_T, S_ψ	Sensitivity functions of torque and flux control loops
		L_m	Mutual inductance
Symbol	**Description**	K_T	Torque constant
R_r	Rotor resistance	ψ_{dr}, ψ_{qr}	d and q components of rotor flux
L_r	Rotor inductance	T_r	Torque reference
i_{ds}, i_{qs}	d and q components of the stator currents	$\overline{\psi}_r$	Flux magnitude reference
T_E	Generated torque	$a_2 = a_1 L_m$	Flux stator current gain
$\overline{\psi}$	Flux magnitude	x_0	Equilibrium value for variable x
a_1	Rotor flux time constant	u_x	Additional control input for variable x
ϕ	Slip angular velocity	σ_r	Rotor resistance perturbation factor
Δx	Deviation from nominal/equilibrium value of variable x	$g_{Td}(s)$	Transfer function $\Delta T_E(s)/\Delta i_{ds}(s)$
		$g_{\psi d}(s)$	Transfer function $\Delta\overline{\psi}^2(s)/\Delta i_{ds}(s)$
δ_x	Perturbation input in variable x	$\gamma(s)$	Multivariable structure function
$g_{Tq}(s)$	Transfer function $\Delta T_E(s)/\Delta i_{qs}(s)$	h_T, h_ψ	Complementary sensitivity of torque and flux control loops
$g_{\psi q}(s)$	Transfer function $\Delta\overline{\psi}^2(s)/\Delta i_{qS}(s)$		
$c : \{in = x, \; out = y\}$	Individual channel using variable y as output and variable x as input.		

have not been fully addressed. Following this line, the main focus of this article is to *comprehensively study the intrinsic dynamical cross-coupling properties of the flux-torque subsystem under typical FOC schemes.* The principal shortcoming of most published works in this regard is that they are focused on the overall control goals and only deal with the cross-coupling as a byproduct (normally direct cancellation methods are applied). For instance, in [16–19] the flux-torque subsystem is analyzed by using local stability concepts and bifurcations. In these references, some aspects of the cross-coupling between the flux and the torque are treated indirectly. Nonetheless, these studies are limited by considering solely equilibrium conditions. In [20] additional aspects of the cross-coupling of this subsystem are used to propose stabilizing controllers. However, the cross-coupling analysis is also limited to equilibrium characteristics and neglects the dynamical aspects. Additional features of flux-torque cross-coupling can be found in classical vector control literature for IMs, such as in [21,22]. Nonetheless, most of these results suffer the same shortcomings as explained before. Ref. [15] successfully presents an approach that considers a current-fed machine and the control of the flux-torque subsystem; however, neither the resulting coupling nor the effect of perturbations over this coupling are discussed. Although the flux-torque subsystem has been extensively studied, the dynamical aspects of its cross-coupling are yet to be addressed.

Interesting results on the flux-torque control problem have been reported using passivity analysis. For instance, in [23,24] multivariable flux-torque controllers and some steady state cross-coupling characteristics are studied. An important conclusion from these works is that that by stabilizing the stator currents with a correct *d-q* alignment the flux error must converge to zero –which is the key for flux-torque decoupling as will be also discussed here. However, the results shown in [23,24] do not allow an easy assessment of the perturbation rejection characteristics of flux–torque controllers due to the inherent cross-coupling, something which is thoroughly covered in this article.

The effects of *perturbations* on the flux-torque cross-coupling are also understudied in the available literature. For example in [28] the flux-torque cross-coupling is successfully eliminated in the presence of perturbations, but the requirements for this to be achieved or the even the mechanisms of how it was achieved are not reported. Fully non-linear controllers have also been developed for IMs. For instance, in [9] a non-linear controller is presented and it is shown that stability can be preserved under certain degree of slip angle deviation. Nonetheless, flux-torque cross-coupling was observed under perturbations, but no additional effort was made to characterize it or eliminate it.

On the other hand, there are several recent theoretical developments for the design of multivariable control systems. For instance, in [25] an observer is proposed to estimate the cross-coupling in real time in order to actively compensate and decouple the system. Following a similar line, in [26] an interesting treatment of active uncertainty compensation and on-line estimation is presented for a class of systems. These ideas are further developed in [27] with good theoretical results. Nonetheless, the adaptation of these theoretical developments to the particular problem at hand (*i.e.* analyzing the flux-torque cross-coupling of IMs when using FOC schemes) requires a significant effort due to the complexity of the theoretical framework. In this context, a simpler framework with accessible tools in an engineering environment would be better suited for a first approach to address this problem.

A widely known tool for studying the cross-coupling of multi-variable systems is the *relative gain array* (RGA) matrix [29,30]. The RGA matrix is normally used for steady state cross-coupling analysis. That is, an in-depth RGA matrix analysis of the flux-torque subsystem may reveal the same results as those already found in the literature. In this context, *individual channel analysis and design* (ICAD) is a framework which goes far beyond the RGA matrix analysis and includes the dynamical effects of the cross-coupling and of closed loop controllers [31]. In this article, the cross-coupling of the flux-torque subsystem is studied under the ICAD framework. By application of ICAD, several novel characteristics of the flux-torque subsystem are revealed and associated to known equilibrium point characteristics. For instance, it is shown that this subsystem has intrinsic stator currents perturbation rejection capabilities. Moreover it is shown that these capabilities are due to the existence of a particular transmission zero in the flux-torque subsystem.

One of the major drawbacks of FOC schemes is their sensitivity to slip angular velocity perturbations. It is also known that these perturbations are related in turn to rotor resistance perturbations. Several studies have been made considering the effect of variations of this parameter in specific control schemes [10,32–34]. In this article, slip angular velocity perturbations modeled as rotor resistance perturbations are considered. The results clearly show the negative impact of these perturbations over the closed loop system through the cross-coupling of the flux and torque.

Finally, some of the most relevant equilibrium point conclusions for the flux-torque subsystem, which are normally scattered among several references, are derived here from first principles and then extended to their dynamical counterpart. Conditions where problems with the equilibrium point arise are addressed. It is shown that these issues appear when flux and torque are

simultaneously controlled in the presence of slip angular velocity deviations. The information presented in this work can help to establish a global view of the flux-torque cross-coupling problem. This may be useful for gaining a better understanding of the process and proposing better control schemes.

2. IM flux-torque model

The well-known IM model expressed in a rotating reference frame is given by [1,21,28,33]:

$$v_{ds} = R_s i_{ds} + \dot{\psi}_{ds} - \eta \psi_{qs}$$
$$v_{qs} = R_s i_{qs} + \dot{\psi}_{qs} + \eta \psi_{ds}$$
$$0 = R_r + i_{dr} + \dot{\psi}_{dr} - (\eta - \omega_r)\psi_{qr}$$
$$0 = R_r + i_{qr} + \dot{\psi}_{qr} + (\eta - \omega_r)\psi_{dr} \tag{1}$$

$$T_E = K_T(\psi_{dr} i_{qs} - \psi_{qr} i_{ds})$$
$$\dot{\omega}_r = \frac{P}{2J}(T_E - T_L)$$

where η is the angular speed of the arbitrary reference frame, v_{ds}, v_{qs} are the d and q components of the stator voltage, i_{ds}, i_{qs} are the d and q components of the stator current, ψ_{dr}, ψ_{qr} are the d and q components of rotor flux, ω_r is the rotor angular velocity, R_r is the rotor resistance, J is the rotor inertia, T_L is an external torque load, P is the number of poles, T_E is the generated torque and $K_T = \frac{3}{2}\left(\frac{P}{2}\right)\frac{L_m}{L_r}$. For consistency, it should be noted that the preferred notation for stationary variables in a number of references employs sub-indices d-q, whereas variables in a rotating frame are denoted with sub-indices x–y [22]. However, the notation here presented is also widely used.

On the other hand, the rotor flux linkages can be expressed as [1,21,33]:

$$\psi_{dr} = L_m i_{ds} + L_r i_{dr}$$
$$\psi_{qr} = L_m i_{qs} + L_r i_{qr} \tag{2}$$

where L_r, L_m are the rotor and mutual inductances respectively.

If the machine is current-fed or if a high-bandwidth control loop over the stator currents is implemented, then the stator currents i_{ds}, i_{qs} can be considered as an input of system (1). In particular, the most common high-performance FOC strategies consist in using a VSI to actuate over the stator currents. With this actuator a control loop over the stator currents is closed with a bandwidth at least one decade greater than the motor synchronous speed. For instance, an IM with nominal electrical speed of 376 rad/s would require a stator currents bandwidth of at least 3700 rad/s. In fact, in [33] it is discussed how this control loop must be designed with the highest bandwidth possible. Conversely, the flux dynamics are governed by the rotor time constant L_r/R_r with bandwidths around 10 rad/s. By comparing the bandwidth of the stator currents control loop with that of the rotor flux it is clear that the slower dynamic can be analyzed separately from the fast dynamic. This strategy is widely used for both FOC [1–3,10,31] and other IM control schemes [11–15] and allows neglecting the stator currents dynamics.

Substituting the rotor flux linkages (2) in system (1) and considering the stator currents as inputs yields:

$$\dot{\psi}_{dr} = a_2 i_{ds} - a_1 \psi_{dr} - (\omega_r - \eta)\psi_{qr}$$
$$\dot{\psi}_{qr} = a_2 i_{qs} - a_1 \psi_{qr} + (\omega_r - \eta)\psi_{dr} \tag{3}$$

$$T_E = K_T(\psi_{dr} i_{qs} - \psi_{qr} i_{ds})$$

$$\dot{\omega}_r = \frac{P}{2J}(T_E - T_L)$$

with $a_1 = \frac{R_r}{L_r}$ and $a_2 = \frac{L_m R_r}{L_r}$.

Since system (3) depends on the angular velocity ω_r the flux-torque subsystem cannot be, in principle, separated from the mechanical equation. However, if ω_r is known and a new arbitrary input variable ϕ such that $\eta = \omega_r + \phi$ is introduced, then the first three equations of model (3) can be re-written as:

$$\dot{\psi}_{dr} = a_2 i_{ds} - a_1 \psi_{dr} + \phi \psi_{qr}$$
$$\dot{\psi}_{qr} = a_2 i_{qs} - a_1 \psi_{qr} - \phi \psi_{dr}$$
$$T_E = K_T(\psi_{dr} i_{qs} - \psi_{qr} i_{ds}) \tag{4}$$

where ϕ is referred to as the slip angular velocity.

Under this setup the flux-torque subsystem can be studied as a process independent of the mechanical subsystem. The resulting system can be analyzed as a *multiple-input-multiple-output* (MIMO) system where the stator currents i_{ds}, i_{qs} and the slip angular velocity ϕ act as inputs and the generated torque T_E and rotor fluxes ψ_{dr}, ψ_{qr} act as outputs.

3. FOC equilibrium point analysis

The equilibrium point of system (4) is fundamental for designing IM control systems. Indeed, the motivating force and strategy behind the design of a control scheme are dependent on the setting of the equilibrium points. For system (4), these are obtained by setting:

$$0 = a_2 i_{ds0} - a_1 \psi_{dr0} + \phi \psi_{qr0}$$
$$0 = a_2 i_{qs0} - a_1 \psi_{qr0} - \phi \psi_{dr0} \tag{5}$$

where x_0 denotes the equilibrium value of variable x (i.e. i_{ds}, i_{qs}, ψ_{ds} or ψ_{qs}).

The main problem arises from the ambiguity of the equilibrium values. It is necessary to select nominal values for two fluxes, two currents and the slip angular velocity in order to generate the torque defined by the last equation of system (4). That is, for the two equations defined by (5) there are five unknowns. As a starting point, this set of equations can be solved for the rotor fluxes in term of the stator currents:

$$\psi_{dr0} = \frac{a_2 \phi_0 i_{qs0} + a_1 a_2 i_{ds0}}{a_1^2 + \phi_0^2}, \quad \psi_{qr0} = \frac{-a_2 \phi_0 i_{ds0} + a_1 a_2 i_{qs0}}{a_1^2 + \phi_0^2} \tag{6}$$

Alternatively, equations in (5) can be also solved for the stator currents in terms of the rotor fluxes:

$$i_{ds0} = \frac{a_1 \psi_{dr0} - \phi_0 \psi_{qr0}}{a_2}, \quad i_{qs0} = \frac{a_1 \psi_{qr0} + \phi_0 \psi_{dr0}}{a_2} \tag{7}$$

A possible solution for finding a feasible set of equilibrium values can be defined by substituting (7) in the last equation of (4); that is:

$$T_{E0} = \frac{K_T \phi_0}{a_2}\left(\psi_{dr0}^2 + \psi_{qr0}^2\right) \tag{8}$$

Let the flux magnitude be defined as $\overline{\psi} = \| \begin{bmatrix} \psi_{dr} & \psi_{qr} \end{bmatrix} \|$. By substituting it in (8), the generated torque in steady state becomes:

$$T_{E0} = \frac{K_T}{a_2}\phi_0 \overline{\psi}_0^2 \tag{9}$$

where both ϕ_0 and $\overline{\psi}_0$ depend on the input variables and can be potentially manipulated via a closed loop controller. However, it is important to note that while $\overline{\psi}$ may be manipulated, it depends on the flux dynamics of the motor. On the other hand, the slip angular velocity ϕ may be considered as an input since its dynamics evolve faster than those of the flux.

Thus, the preferred option for manipulating T_E, is to fix $\overline{\psi}$ (i.e. $\overline{\psi}(t) = \overline{\psi}_0$) and use ϕ as an input variable. In reality ϕ is not directly actuated, but depends on the stator currents control loop

which has a much higher bandwidth than the flux-torque subsystem.

3.1. Constant or slowly varying flux magnitude schemes

The flux magnitude can be manipulated in order to improve the motor performance. This has been achieved in [15,16], where the motor torque is maximized by adjusting the values of the flux. In general, the bandwidth of the flux dynamics is lower than that of the torque. This characteristic can be considered for simplifying the analysis of the torque production.

In particular, if the flux magnitude is considered equal to a constant reference $\overline{\psi}_r$ (i.e. $\overline{\psi}_0 = \overline{\psi}_r$), then it is clear from (9) that *the only possible option* for delivering the demanded torque in steady state is by driving the slip angular velocity to:

$$\phi = \frac{a_2 T_r}{\overline{\psi}_r^2 K_T} \tag{10}$$

Eq. (10) represents a fundamental relationship of control schemes based on constant or slowly-varying flux magnitude, and its relationship with classical indirect FOC (IFOC) will be shown in the following paragraphs. It is important to note that most control strategies belong to this classification because the open loop dynamics of the flux are much slower than the stator currents and the torque response time. Closed loop modification of the flux dynamics, for instance by reducing its response time, is physically limited by the actuator constraints; therefore the flux dynamics tend to remain slower than stator currents or torque dynamics even in closed loop operation.

On the other hand, the flux magnitude in steady state conditions is defined by Eq. (6). Therefore, the steady state expression of $\overline{\psi}$ results:

$$\overline{\psi}_0 = \frac{a_2}{\sqrt{a_1^2 + \phi_0^2}} \sqrt{i_{ds0}^2 + i_{qs0}^2} \tag{11}$$

Thus, by combining Eqs. (10) and (11) all possible input combinations satisfying $\overline{\psi}_0 = \overline{\psi}_r$ and $T_{E0} = T_r$ can be calculated with:

$$\sqrt{i_{ds0}^2 + i_{qs0}^2} = \sqrt{\frac{\overline{\psi}_r^2 a_1^2}{a_2^2} + \frac{T_r^2}{\overline{\psi}_r^2 K_T^2}} \tag{12}$$

The solutions of Eq. (12) for i_{ds0} and i_{qs0}, in combination with the slip angular velocity (10), are the set of values for the stator currents which are able to produce the desired torque and flux in steady state. This is an important result since it shows that there are infinite possible combinations and, therefore, an infinite number of possible control schemes exist. One particular scheme is obtained by the direct solution of eq. (12):

$$i_{ds} = \frac{\overline{\psi}_r a_1}{a_2}, \quad i_{qs} = \frac{T_r}{\overline{\psi}_r K_T} \tag{13}$$

The combination of (13) and (10) yields the inputs for the classical IFOC equations. In this case the slip angular velocity reduces to the well-known:

$$\phi = \frac{a_2}{\overline{\psi}_r} i_{qs} \tag{14}$$

Nonetheless, it should be observed that this is not the only stator currents combination that yields the desired flux magnitude and torque in steady state. For instance, another possible solution for Eq. (12) is:

$$i_{qs} = 0, \quad i_{ds} = \sqrt{\frac{\overline{\psi}_r^2 a_1^2}{a_2^2} + \frac{T_r^2}{\overline{\psi}_r^2 K_T^2}} \tag{15}$$

The inputs defined by Eqs. (10) and (13) are fundamental to FOC approaches. This alternative is considered as a *decoupling* solution since i_{ds} depends only on the flux magnitude reference and i_{qs} depends on the torque reference. That is, IFOC inputs yield a flux-producing current i_{ds} and a torque-producing current i_{qs} that are seemingly decoupled. Although FOC schemes are devised specifically for flux-torque decoupling, it will be shown later in the article that the use of FOC schemes in fact *introduces interesting internal coupling characteristics*.

4. Perturbed FOC flux-torque control

In this section the typical IFOC scheme defined by (10) and (13) while considering perturbations is analyzed. A deviation of the nominal steady state can be studied by considering deviations on the system inputs, which for the classical IFOC scheme are given by the stator currents; that is:

$$i_{ds}(t) = \frac{\tilde{a}_1}{\tilde{a}_2}\psi_r + \Delta i_{ds}, \quad i_{qs}(t) = \frac{T_r}{\overline{\psi}_r \tilde{K}_T} + \Delta i_{qs} \tag{16}$$

where Δx denotes a small deviation from the equilibrium point of variable x (i.e. i_{ds} or i_{qs}) and $\tilde{a}$ denotes the estimation of parameter a (i.e. a_1, a_2 or K_T). In other words, each input current is decomposed into a nominal FOC input plus a deviation. Deviations Δx can be used to model perturbations and additional control inputs. For example, variable x (i.e. i_{ds} or i_{qs}) could be defined as $x = u_{foc} + \Delta x$, where u_{foc} is the nominal FOC input for this variable; additionally, $\Delta x = u_x + \delta_x$, where δ_x is a perturbation signal and u_x is an additional control signal. For the slip angular velocity only parametric uncertainty will be considered, therefore:

$$\phi(t) = \frac{\tilde{a}_2 T_r}{\overline{\psi}_r^2 \tilde{K}_T} \tag{17}$$

Inputs (16)–(17) consider parametric uncertainty on the motor parameters, arbitrary perturbation inputs over the stator currents and the existence of additional control inputs over the stator currents.

The rotor resistance represents one of the most important sources for parametric perturbations because variations of this parameter are associated to deviations of the ideal slip angular velocity. Therefore, rotor resistance perturbations will be considered in this article for the study of the cross-coupling of the flux-torque subsystem.

Let the *rotor resistance perturbation factor* σ_r be defined as $\sigma_r = \tilde{R}_r / R_r$, where $\tilde{R}_r$ is the nominal (estimated) rotor resistance and R_r denotes the real rotor resistance. If the values of $a_1 = R_r / L_r$ and $a_2 = (L_m R_r)/L_r$ are considered in (13), it can be observed that the stator currents of a FOC controller are not affected by rotor resistance perturbations –contrary to the slip angular velocity, which may be affected by these perturbations as it can be easily noted from (17). In this case, $\phi(t) = \sigma_r a_2 T_r/(\overline{\psi}_r^2 K_T)$.

According with the discussion of the last paragraphs, if a FOC torque controller is employed under the presence of rotor resistance perturbation, perturbation inputs on the stator currents and additional control inputs for the stator currents, then the inputs for the flux-torque subsystem can be expressed as:

$$i_{ds}(t) = \frac{a_1}{a_2}\overline{\psi}_r + \delta_{ids} + u_{ids}, \quad i_{qs}(t) = \frac{T_r}{\overline{\psi}_r K_T} + \delta_{iqs} + u_{iqs}, \quad \phi(t) = \frac{\sigma_r a_2 T_r}{\overline{\psi}_r^2 K_T} \tag{18}$$

Under these conditions the resulting torque and flux outputs can be studied using linear approximations of (4), with

Current-Fed Non-linear model + perturbed FOC control + stator currents perturbations + external control inputs
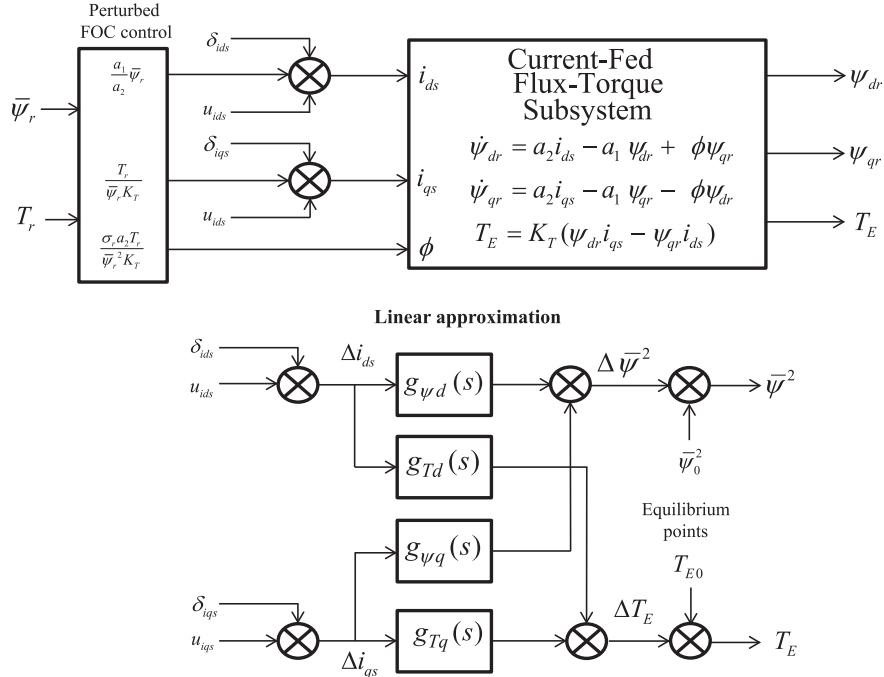

Fig. 1. Current-fed flux-torque subsystem with perturbed FOC control, stator currents perturbations and external control inputs.

Current-Fed Non-linear model + perturbed FOC control + stator currents perturbations + external flux controller
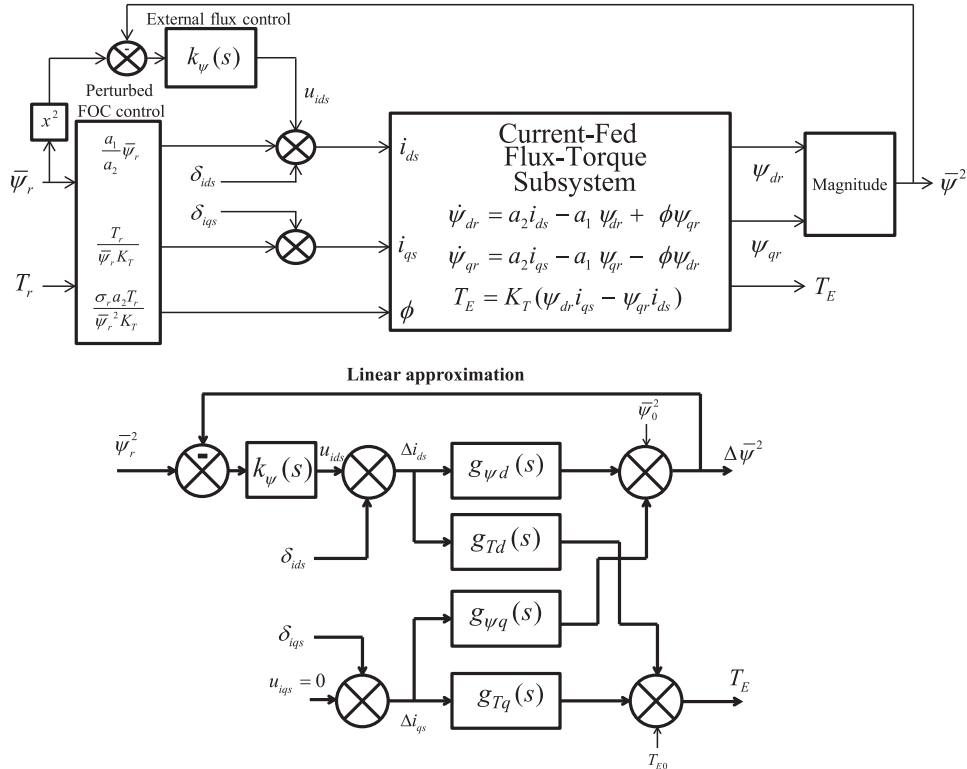

Fig. 2. Current-fed flux-torque subsystem with perturbed FOC control, stator currents perturbations and external flux controller.

equilibrium points (6), and also the following equilibrium inputs:

$$i_{ds0} = \frac{a_1}{a_2}\overline{\psi}_{r0}, \quad i_{qs0} = \frac{T_{r0}}{\overline{\psi}_{r0}K_T}, \quad \phi_0 = \frac{\sigma_r a_2 T_{r0}}{\overline{\psi}_{r0}^2 K_T} \qquad (19)$$

Substitution of eq. (19) into (6) yields the flux equilibrium point of the FOC controller subjected to rotor resistance perturbations:

$$\psi_{dr0} = \frac{\overline{\psi}_{r0}^4 K_T^2 + L_m^2 T_{r0}^2 \sigma_r}{\overline{\psi}_{r0}^4 K_T^2 + L_m^2 T_{r0}^2 \sigma_r^2}\overline{\psi}_{r0}, \quad \overline{\psi}_{qr0} = \frac{\overline{\psi}_{r0}^3 K_T L_m T_{r0}(1-\sigma_r)}{\overline{\psi}_{r0}^4 K_T^2 + L_m^2 T_{r0}^2 \sigma_r^2} \qquad (20)$$
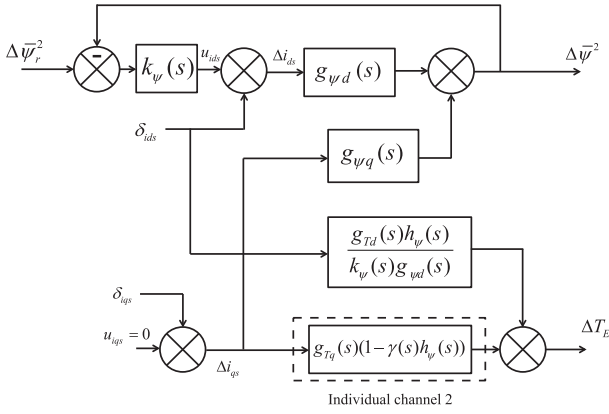
Fig. 3. Flux-torque subsystem with perturbed FOC control, stator currents perturbations and external flux controller using individual channel equivalent.
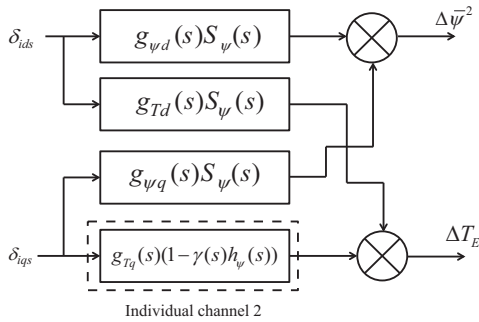

Fig. 4. Perturbation rejection characteristics of the flux-torque subsystem with perturbed FOC control, stator currents perturbations and external flux control.
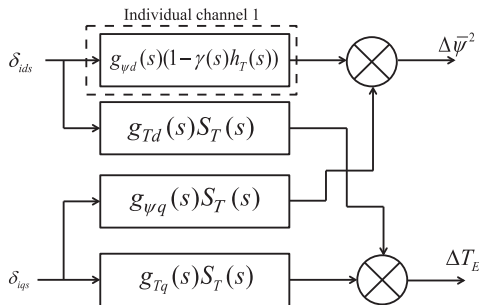

Fig. 5. Perturbation rejection characteristics of the flux-torque subsystem with perturbed FOC control, stator currents perturbations and external torque control.

It can be noticed from (20) that if $\sigma_r = 1$ (*i.e.* no perturbation on the rotor resistance or slip angular velocity) then $\psi_{qr0} = 0$, $\psi_{dr0} = \overline{\psi}_{r0}$ and the steady state flux magnitude is equal to the flux reference. In the same vein, the steady state torque can be obtained by substituting (19)-(20) into (8):

$$T_{E0} = \frac{\sigma_r T_{r0}}{\overline{\psi}_{r0}^2} \frac{\left(\overline{\psi}_{r0}^4 K_T^2 + L_m^2 T_{r0}^2 \sigma_r\right)^2 \overline{\psi}_{r0}^2 + \left(\overline{\psi}_{r0}^3 K_T L_m T_{r0}(1-\sigma_r)\right)^2}{\left(\overline{\psi}_{r0}^4 K_T^2 + L_m^2 T_{r0}^2 \sigma_r^2\right)^2}$$

(21)

Similarly, if $\sigma_r = 1$ then the steady state torque will be equal to the torque reference, *i.e.* $T_{E0} = T_{r0}$.

It is also clear that when $\sigma_r \neq 1$ the resulting steady state torque and flux do not converge to the desired references. However, one may wonder if it is possible to introduce an external correction through the stator currents so that both the flux and the torque converge. In the next sections it will be demonstrated that there is an intricate relationship between flux and torque which

makes it *impossible to correct both flux and torque without correcting the slip*. This will be shown to be the case not only in steady state, but also dynamically. In addition, it will be demonstrated that this phenomena is *due to the existence of a transmission zero present in the flux-torque subsystem*. Moreover, this characteristic introduces unique perturbation rejection characteristics which can be exploited for controller design.

5. Flux-torque cross-coupling case 1: unperturbed rotor resistance

The case without rotor resistance perturbation is analyzed first; that is, $\sigma_r = 1$. Here the equilibrium point corresponds to the nominal FOC equilibrium defined by $\psi_{qr0} = 0$, $\psi_{dr0} = \overline{\psi}_{r0}$ and $T_{E0} = T_{r0}$.

As discussed in Section 3, the FOC input currents are considered as a decoupling solution for the flux-torque subsystem. In particular, current i_{ds} is considered as an input of the flux dynamics whereas i_{qs} is considered as an input of the torque dynamics. This fact was confirmed by the equilibrium point analysis of Section 3 (Eqs. (12)–(13) and their discussion). In order to determine the dynamical effects of such condition the following input-output pairings will be considered:

$$c_1 : \left\{ in = u_{ids}, out = \overline{\psi}^2 \right\}$$
$$c_2 : \left\{ in = u_{iqs}, out = T_E \right\}$$

(22)

where c_1 and c_2 are called *individual channels* and represent the input-output relationship between the specified input-output pairings. In particular, the notation $c_i : \left\{ in = x, out = y \right\}$ will be used along the article to denote that input x is used to drive output y. In addition, the square of the flux magnitude $\overline{\psi}^2$ will be used as an output to simplify the analysis.

A linear approximation of the flux-torque subsystem using the input-output pairings defined by (22) yields:

$$\dot{x} = Ax + Bu$$
$$y = Cx + Du$$

(23)

where the state, input and output vectors are given by $x = \begin{bmatrix} \Delta\psi_{dr} & \Delta\psi_{qr} \end{bmatrix}^T$, $u = \begin{bmatrix} \Delta i_{ds} & \Delta i_{qs} \end{bmatrix}^T$ and $y = \begin{bmatrix} \Delta\overline{\psi}^2 \Delta T_E \end{bmatrix}^T$ respectively. The state space matrices of system (23) are given by:

$$A = \begin{bmatrix} -a_1 & \phi_0 \\ -\phi_0 & -a_1 \end{bmatrix} \quad B = \begin{bmatrix} a_2 & 0 \\ 0 & a_2 \end{bmatrix} \quad C = \begin{bmatrix} 2\psi_{dr0} & 2\psi_{qr0} \\ K_T i_{qs0} & -K_T i_{ds0} \end{bmatrix}$$
$$D = \begin{bmatrix} 0 & 0 \\ -K_T\psi_{qr0} & K_T\psi_{dr0} \end{bmatrix}$$

(24)

The equilibrium points for system (23) are obtained considering the perturbed FOC controller described in Section 4, which can be calculated using Eqs. (6) and (19).

System (23) is represented in the frequency domain as:

$$\begin{bmatrix} \Delta\overline{\psi}^2(s) \\ \Delta T_E(s) \end{bmatrix} = \begin{bmatrix} g_{\psi d}(s) & g_{\psi q}(s) \\ g_{Td}(s) & g_{Tq}(s) \end{bmatrix} \begin{bmatrix} \Delta i_{ds}(s) \\ \Delta i_{qs}(s) \end{bmatrix}$$

(25)

Fig. 1 shows a block diagram of the flux-torque subsystem using the FOC controller and its linear approximation using system (25). Note that the *transfer function matrix* (TFM) (25) is the linear approximation of the flux-torque subsystem *including the perturbed FOC controller*.

Although the IFOC scheme studied in the last section aims to manipulate the flux and torque levels directly, it is common practice to use additional control loops to further regulate these variables; *direct* FOC (DFOC) belongs to this kind of schemes. Fig. 2 shows the resulting configuration when an external flux controller

$k_\psi(s)$ is used for individual channel c_1: $\{in = u_{ids}, \ out = \overline{\psi}^2\}$. Note that in this case the additional control input for current i_{qs} is not used, *i.e.* $u_{iqs} = 0$, but there are perturbations present in both stator currents.

The torque response can be also regulated with an external torque controller $k_T(s)$ using individual channel c_2 : $\{in = u_{iqs}$, $out = T_E\}$. The design of the external controllers $k_\psi(s)$, $k_T(s)$, and the analysis of the closed loop perturbation rejection characteristics require the study of the dynamical properties of system (25).

System (25) is a 2×2 MIMO system which can be analyzed in the context of *ICAD*. ICAD is a theoretical framework which allows the analysis of MIMO systems using *single input single output* (SISO) and frequency analysis concepts [35,36]. The key element of ICAD is the *multivariable structure function* (MSF). This frequency domain function is inherent to the nature of the process. Its appropriate interpretation reveals important dynamical characteristics regarding the cross-coupling of the individual channels, including the transmission zeros, the existence of stabilizing controllers and the robustness characteristics of the closed loop control system. Some examples of the application of ICAD concepts to electrical machines can be found in [37–40].

With no rotor resistance perturbation, *i.e.* $\sigma_r = 1$, the MSF of (25) is expressed as:

$$\gamma(s) = \frac{g_{\psi q}(s) g_{Td}(s)}{g_{\psi d}(s) g_{Tq}(s)}$$

$$= \frac{a_2{}^2 T_{r0}{}^2 s + 2a_1 a_2{}^2 T_{r0}{}^2}{\overline{\psi}_{r0}{}^4 K_T{}^2 s^3 + (2a_1 \overline{\psi}_{r0}{}^4 K_T{}^2) s^2 + (2a_2{}^2 T_{r0}{}^2 + \overline{\psi}_{r0}{}^4 K_T{}^2 a_1{}^2) s + 2a_1 a_2{}^2 T_{r0}{}^2} \tag{26}$$

For a 2×2 system, it can be shown that if individual channel c_2 : $\{in = u_{iqs}, \ out = T_E\}$ is closed then [35,36]:

$$\frac{\Delta \overline{\psi}^2(s)}{\Delta i_{ds}(s)} = g_{\psi d}(s) \left(1 - \gamma(s) \frac{k_T(s) g_{Tq}(s)}{1 + k_T(s) g_{Tq}(s)} \right) \tag{27}$$

Conversely, if individual channel c_1 : $\{in = u_{ids}, \ out = \overline{\psi}^2\}$ is closed then:

$$\frac{\Delta T_E(s)}{\Delta i_{qs}(s)} = g_{Tq}(s) \left(1 - \gamma(s) \frac{k_\psi(s) g_{\psi d}(s)}{1 + k_\psi(s) g_{\psi d}(s)} \right) \tag{28}$$

It is interesting to note that the closed loop complementary sensitivity of $k_T(s) g_{Tq}(s)$ and $k_\psi(s) g_{\psi d}(s)$ can be easily identified in eqs. (27)–(28); thus, it is convenient to express them as:

$$\frac{\Delta \overline{\psi}^2(s)}{\Delta i_{ds}(s)} = g_{\psi d}(s)(1 - \gamma(s) h_T(s)), \quad \frac{\Delta T_E(s)}{\Delta i_{qs}(s)} = g_{Tq}(s)(1 - \gamma(s) h_\psi(s)) \tag{29}$$

with $h_T(s) = k_T(s) g_{Tq}(s) / \left(1 + k_T(s) g_{Tq}(s) \right)$ and $h_\psi(s) = k_\psi(s) g_{\psi d}(s) / \left(1 + k_\psi(s) g_{\psi d}(s) \right)$.

Eq. (29) are the resulting input-output relationships when either the flux or the torque control loops are closed and are also denoted as individual channels 1 and 2 respectively. For instance, if *only* the flux control loop is closed with an external controller $k_\psi(s)$, and defining $\Delta \overline{\psi}_r^2 = \overline{\psi}_r^2 - \overline{\psi}_0^2$, then the resulting configuration shown in Fig. 3 is obtained.

5.1. Perturbation rejection

The perturbation rejection characteristics can be studied by isolating the effects of the perturbation inputs δ_{ids}, δ_{iqs} and by defining the sensitivity function as:

$$S_\psi(s) = \frac{1}{1 + k_\psi(s) g_{\psi d}(s)} \tag{30}$$

If (30) is considered, the diagram of Fig. 3 can be reformulated as the one shown in Fig. 4.

From Fig. 4 it is clear that the flux control loop is able to reject perturbations from both δ_{ids} and δ_{iqs} through the flux control loop sensitivity function $S_\psi(s)$. Notice that the torque is operating in open loop and is also subject to the perturbations. Two important observations can be made. The first one is that the torque is also able to reject perturbations δ_{ids} through the sensitivity of the flux control loop. The second observation, and one of the key results of the article, is that the open loop variable has also perturbation rejection characteristics which are defined by the open loop individual channel Eqs. (27) and (28). Note that in this example the flux control loop has been closed; alternatively, the torque loop may be closed and then the flux would operate in open loop. In this case the resulting perturbation rejection configuration is summarized by Fig. 5.

It should be emphasized that while the sensitivity function analysis is well-known and needs no further description, the analysis of the individual channel characteristics in the context of open loop perturbation rejection is non-existent in the current literature. This is assessed in detail next.

The structure of eqs. (27)-(28) has several special characteristics which are noteworthy. If a high-bandwidth controller (for either the flux or the torque) is considered then $h_\psi(s) \approx 1$ or $h_T(s) \approx 1$. Therefore, the open loop individual channel equations become $g_{\psi d}(s)(1 - \gamma(s))$ and $g_{Tq}(s)(1 - \gamma(s))$. In the previous equations the factor $(1 - \gamma(s))$ contains information regarding the maximum attainable perturbation rejection characteristics through the use flux or torque controllers. For example, if a *perfect* control for flux is used then $h_\psi(s) \approx 1$ and $S_\psi(s) \approx 0$ [30,41]. In this case, by examining Fig. 4 it is clear that the flux control loop is able to reject perturbations from both stator currents (*i.e.* δ_{ids} and δ_{iqs}). Regarding the torque, perturbations δ_{ids} are also rejected through
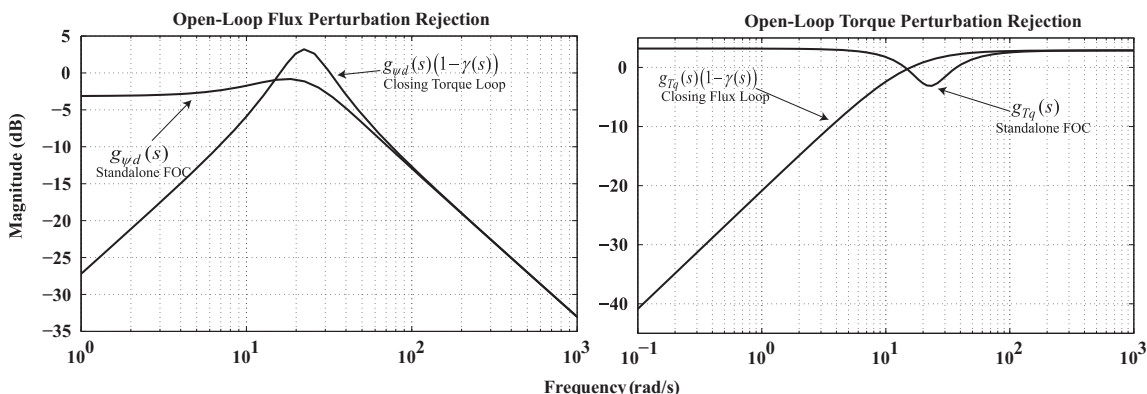

Fig. 6. Comparison of the open loop perturbation rejection characteristics for the flux and torque.

the flux control loop sensitivity, whereas a perturbation rejection element for δ_{iqs} also exists, given by $(1-\gamma(s))$. Therefore, if a *perfect* control for flux is attained, then a perfect perturbation rejection of δ_{iqs} at an arbitrary frequency ω_0 for the torque would require that $\gamma(j\omega_0) = 1$. This conclusion is more relevant in light of the following facts, which are known through ICAD theory [35]:

- The transmission zeros of a MIMO system are related to $\gamma(s)$; note that for a 2×2 MIMO system $1 - \gamma(s) = \det[G(s)] = g_{11}(s) g_{22}(s) - g_{12}(s)g_{21}(s)$.
- *The condition $\gamma(j\omega_0) = 1$ indicates the existence of a transmission zero on the imaginary axis at frequency ω_0 rad/s.*

The transmission zeros are the multivariable equivalent of the zeros from SISO systems. It is not necessary for the scalar transfer functions of a TFM to have zeros for the system to have transmission zeros. In addition, the transmission zeros correspond to the linearization of the internal dynamics of a non-linear system. Normally, the transmission zeros are crucial to determine the existence of stabilizing controllers for a certain set of control specifications. For instance, transmission zeros in the right half of the complex plane (non-minimum phase zeros) are indicative of limitations on the attainable bandwidth. In the context of the problem at hand, it is notable that the presence of transmission zeros near the imaginary axis in system (25) are indicative of increased perturbation rejection characteristics.

Table 1
Typical IM parameters [42]

Parameter	Value	Parameter	Value
R_s	16.2 Ω	L_r	1.49 H
R_r	23 Ω	L_m	1.41 H
L_s	1.44 H	P	2

Table 2
Control specifications for the external flux and torque controllers

Specification	Flux	Torque
Bandwidth	40 rad/s	100 rad/s
Phase Margin	> 50°	> 50°
Gain Margin	> 12 dB	> 12 dB

Recalling Eq. (26), it is clear that $\gamma(0) = 1$. Therefore, according to the conclusions of the last paragraph:

- System (25) has a transmission zero at $\omega_0 = 0$. This can be confirmed by calculating the Smith-McMillan [30] form of (25) (omitted here for brevity).
- A stabilizing high steady-state gain controller for either the flux *or* the torque channel is sufficient to achieve perfect stator currents perturbation rejection for both the flux and the torque in the steady state. For example, if the flux channel is closed with a controller including integral effect this implies $h_\psi(0) \approx 1$ and $S_\psi(0) \approx 0$. In addition, $\gamma(0) = 1$ implies that $(1 - \gamma(0)h_\psi(0)) \approx 0$. Considering Fig. 4, then it is clear that both perturbations δ_{ids} and δ_{iqs} can be rejected for both the flux and the torque.

The previous steady-state conclusions can be extended to all frequencies using typical Bode diagrams. Fig. 6 shows the resulting perturbation rejection characteristics of $g_{\psi d}(s)(1-\gamma(s))$ and $g_{Tq}(s)(1-\gamma(s))$. A typical IM with the parameters described in Table 1 has been considered, with nominal equilibrium torque and flux references of 1 Nm and 1 Wb respectively. Fig. 6 also shows the open loop response to the perturbation inputs, *i.e.* using only FOC. The tradeoffs of closing either the flux or the torque control loop are readily visible in this figure, summarized next:

- Closing the flux control loop results in good perturbation rejection for the torque only for low frequencies.
- Closing the torque control loop results in good perturbation rejection for the flux for both low and high frequencies. However, there is a frequency band in which the perturbations are amplified.

It is important to note that the *open loop* perturbation rejection characteristics shown in Fig. 6 consider either a flux or a torque controller of infinite bandwidth. That is, it is not possible to make further improvements by enhancing these controllers. For a more realistic example consider the following flux and torque controllers:

$$k_\psi(s) = \frac{100(s+20)}{s(s+50)}, \quad k_T(s) = \frac{21978(s+75)}{s(s+8)(s+350)} \quad (31)$$

These controllers were designed using classical *Bode shaping* techniques with the specifications indicated in Table 2, which can be considered as high-performance for typical IMs. The plants
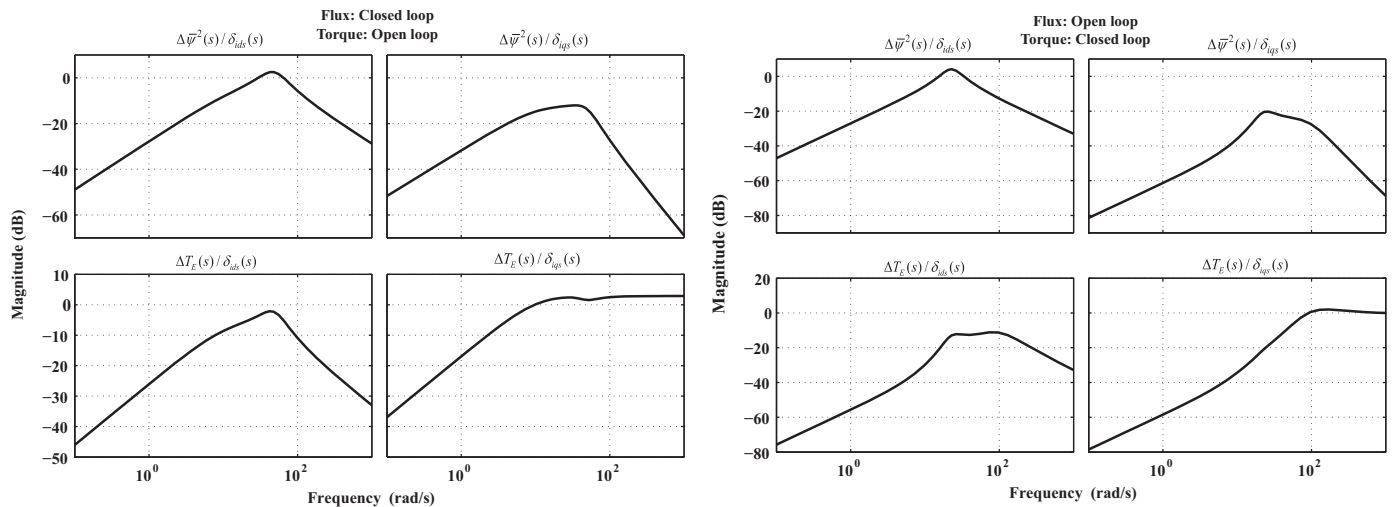

Fig. 7. Stator currents perturbations rejection perturbation characteristics of the flux-torque subsystem using external flux or torque controllers (31).
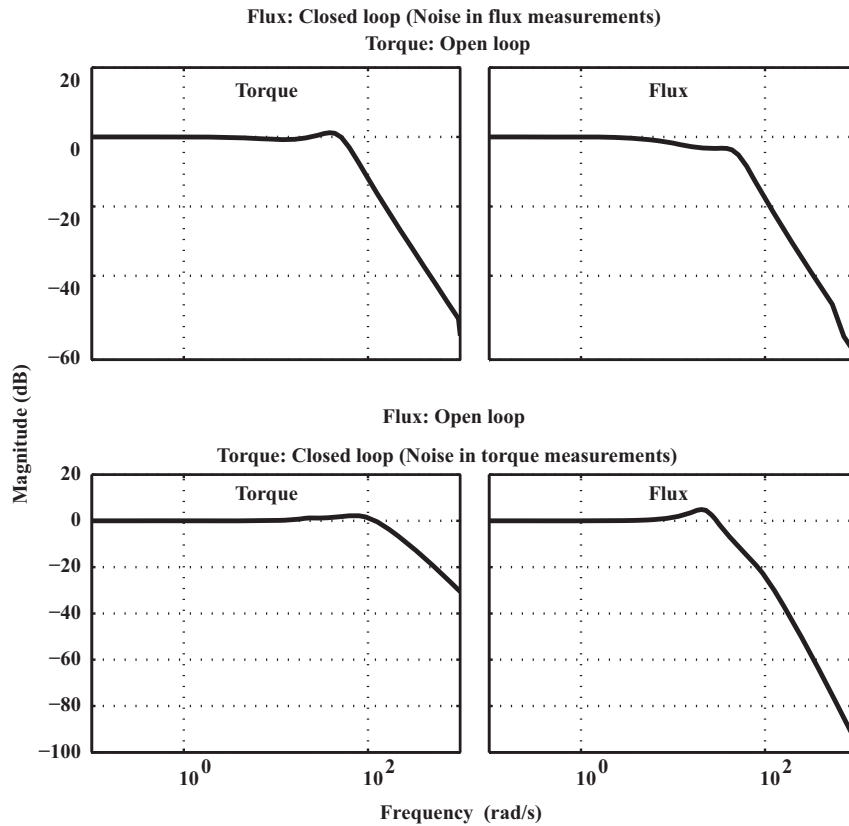
Fig. 8. Sensor noise rejection characteristics of the flux-torque subsystem using external flux or torque controllers (31).
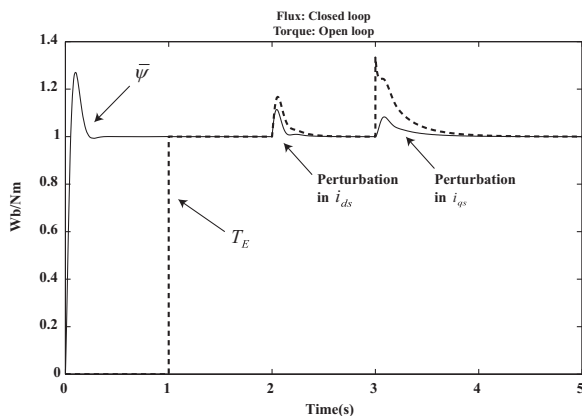

Fig. 9. Simulated flux and torque responses considering no rotor resistance perturbations and an external flux controller.
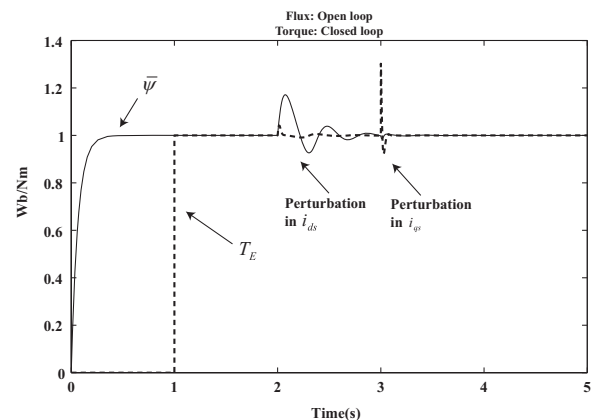

Fig. 10. Simulated flux and torque responses considering no rotor resistance perturbations and an external flux controller.

used for the design of controllers (31) where $g_{\psi d}(s)$ and $g_{Tq}(s)$ respectively.

The resulting perturbation rejection characteristics of the flux-torque subsystem employing controllers (31) are summarized in Fig. 7. These characteristics can be used to determine which control scheme is the best suited for a particular set of control specifications and operating conditions. For example, consider that the torque loop is closed and the flux is operated in open loop (the second case of Fig. 7); in this condition the effect of perturbation δ_{ids} is worst around 22 rad/s, but for all other cases the perturbation rejection level is good. On the other hand, recall that δ_{ids} models a perturbation on the stator currents, and normally the stator currents are operated by an internal high-bandwidth controller [39]. Therefore,

if the stator currents subsystem is designed so that δ_{ids} is low around 22 rad/s then the flux-torque subsystem will achieve a good overall level of perturbation rejection. This shows how the flux-torque subsystem sensitivity characteristics can be translated into specifications for other IM subsystems in order to achieve better global results.

5.2. Sensor noise

In general, it is common to consider noise as either input perturbations or sensor noise. The main focus of the article is to study the effect of stator currents perturbations, which in this context act as input perturbations. Nonetheless, the issue of sensor noise is briefly discussed in this section for completeness.
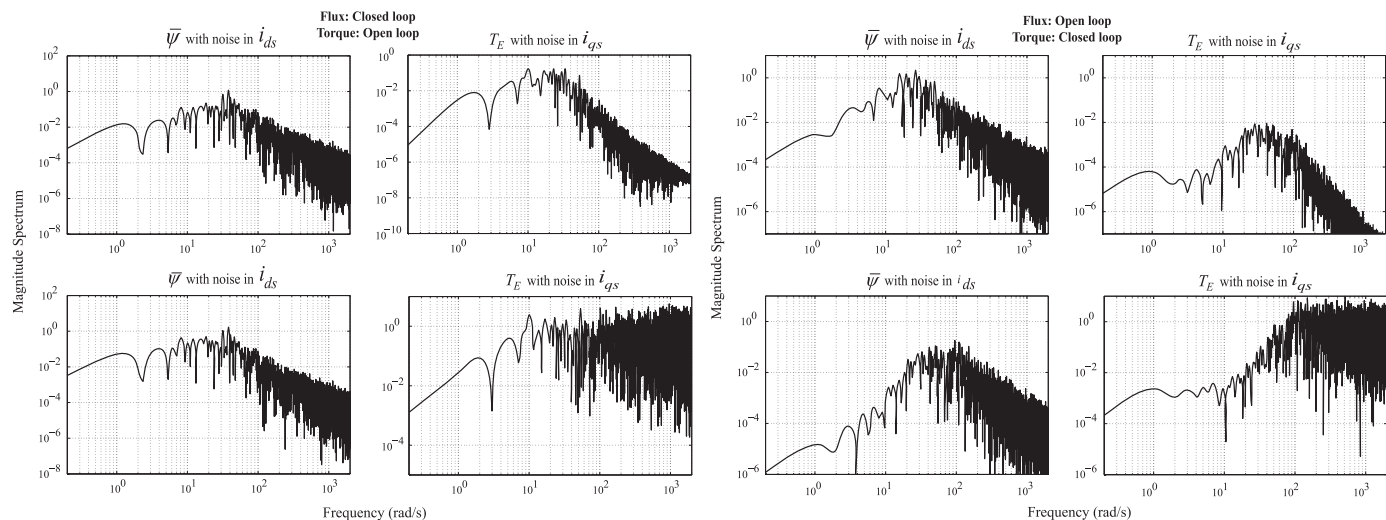
Fig. 11. Magnitude spectrum of the torque and flux using external flux or torque controllers (31) considering pseudo white noise stator currents perturbations.

Consider the decomposition shown in Fig. 2. If the flux is operated in closed loop, then the flux and torque responses due to flux sensor noise are given by $k_\psi(s)g_{\psi d}(s)/\left(1+k_\psi(s)g_{\psi d}(s)\right)$ and $-k_\psi(s)g_{Td}(s)/\left(1+k_\psi(s)g_{\psi d}(s)\right)$ respectively. Conversely, if the torque loop is closed then the torque and flux responses due to torque sensor noise yield $k_T(s)g_{Tq}(s)/\left(1+k_T(s)g_{Tq}(s)\right)$ and $-k_T(s)g_{\psi q}(s)/\left(1+k_T(s)g_{Tq}(s)\right)$. This indicates that the effect of sensor noise can be modeled with the complementary sensitivity, which is incidentally the same as in classical SISO configurations [30,41].

The sensor perturbation rejection characteristics for the machine characterized in Table 1 with controllers (31) are shown in Fig. 8. From this figure it can be observed that the effect of sensor noise on the flux or torque measurements (or observer estimation error) is akin to the complementary sensitivity function, which confirms the discussion of the last paragraph. In particular, the system cannot reject low frequency noise (lower than the closed loop bandwidth), but is able to reject higher frequency noise (higher than the closed loop bandwidth). By observing both Figs. 7 and 8, it can be appreciated that the classical conclusion of the combined sensitivity and complementary sensitivity also applies here: the system is most sensible to perturbations/noise around the bandwidth frequency. It is worth noticing that the flux sensor noise has an effect over the system only when the flux control loop is closed whereas the torque sensor has an effect only when the torque loop is closed. Since the treatment of sensor noise in these conditions is well-known, no further discussion is warranted.

5.3. Time domain characteristics

Non-linear digital simulations were carried out to confirm the perturbation rejection characteristics discussed in the last section. All simulations were performed using MATLAB-Simulink™ with a variable-step Dormand-Prince solver and a relative tolerance of 10^{-6}. In addition, initial conditions for all variables were set to zero. Fig. 9 shows a simulation of the control system of Fig. 2 using the non-linear model (4), the parameters of Table 1 and flux controller (31). References of 1 Nm and 1 Wb were used for the torque and the flux respectively. The torque reference was kept at zero until $t=1$ so that the flux stabilized; this allows to verify the level of

flux-torque coupling. In this case it is clear that the torque is fully decoupled from the flux since the torque response is almost instantaneous without affecting the flux. Such a response occurs since no perturbation in the slip angular velocity was considered; i.e. $\sigma_r = 1$. Step perturbations to the stator currents i_{ds} and i_{qs} were simulated at 2 and 3 s. The amplitude of these perturbations was a third of the nominal value for each current.

By observing the results in Fig. 9 it can be concluded that the perturbation rejection characteristics predicted by the analysis of the last section have been confirmed. In particular, it can be noticed that the torque is able to reject perturbations from both stator currents even if it is operating in open loop.

An additional simulation was carried out with the flux operating in open loop and the torque operating in closed loop, with results shown in Fig. 10. Torque controller (31) has been used, with all other conditions kept as in the previous simulation.

As it can be observed from Fig. 10, the flux is also able to reject perturbations from both stator currents. In addition, the overall performance of the system is better due to the higher bandwidth used in the torque control loop. This allows concluding that it is recommendable to control the torque channel (i.e. $in = u_{iqs}$, $out = T_E$) while maintaining the slip angular velocity the closest possible to (10) (this last requirement will be more evident from the results of the next section). The design of linear and robust controllers closing the torque channel has been theoretically and experimentally studied previously [32].

5.4. Time dependent perturbations

In order to complement the constant perturbation assessment of the previous section, time dependent perturbations in the stator currents were considered. This study shows that the frequency analysis of Section 5.1, which was developed by means of linear approximations, is fairly accurate in predicting the perturbation rejection behavior of the non-linear FOC flux-torque subsystem.

Digital simulations in the same conditions as those summarized by Figs. 9 and 10 were performed. In this case a pseudo white noise was considered as perturbation in either i_{ds} or i_{qs} so as to isolate the effect of each stator current perturbation. The noise signal was obtained with a random number generator with normal distribution, sample time of 0.001 s and an average power of 0.01. The spectrum of the flux and torque signals was calculated using the Fast Fourier Transform with a buffer of 14 bits. The resulting
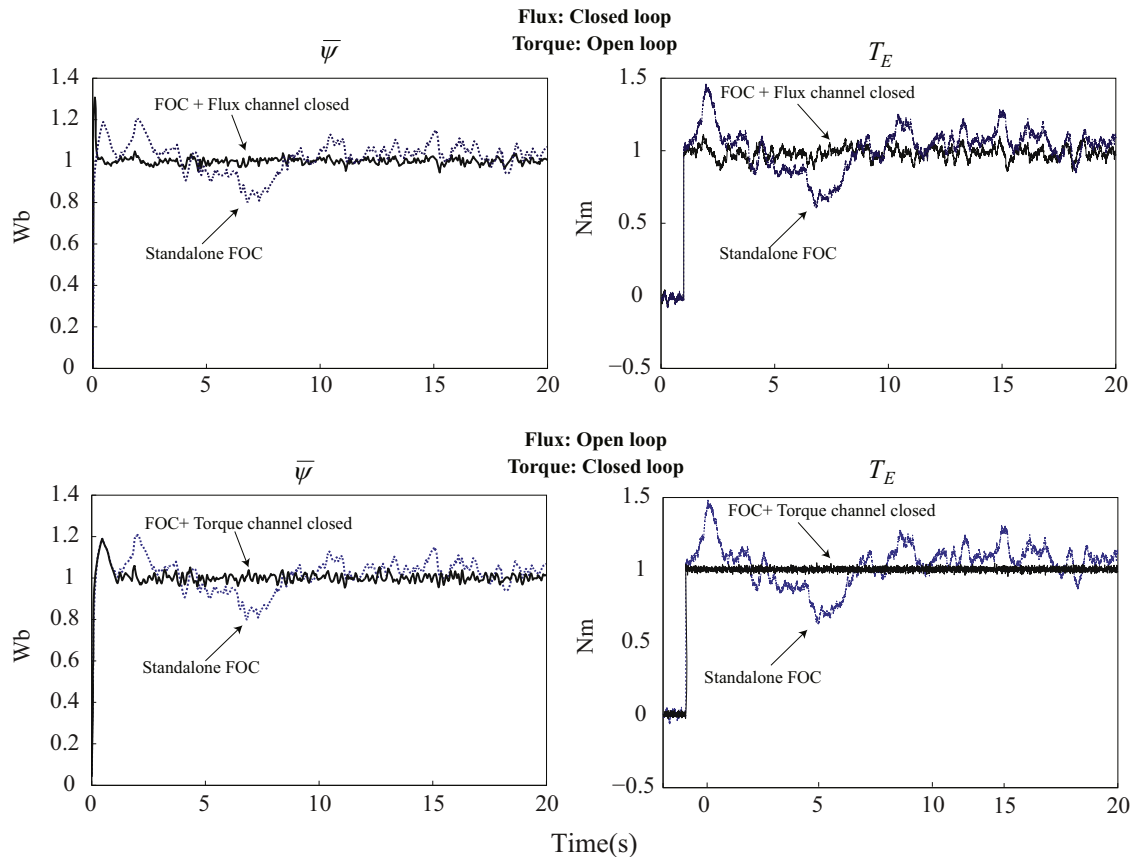
Flux: Closed loop
Torque: Open loop

Fig. 12. Simulated flux and torque responses considering colored noise perturbations in the stator currents.
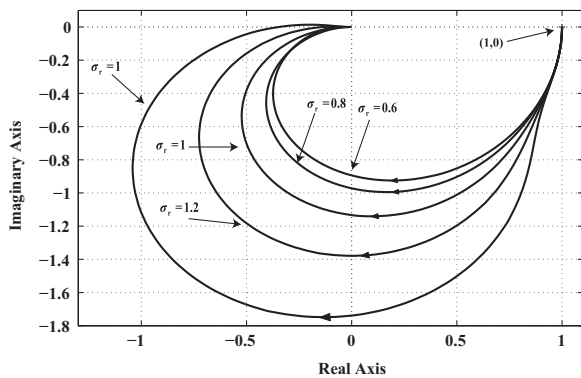

Fig. 13. MSF of the flux-torque subsystem considering the stator currents as inputs and a FOC controller with rotor resistance perturbations.

magnitude spectra of these simulations are shown in Fig. 11. This figure is directly comparable with Fig. 7, which shows the perturbation rejection characteristics predicted by the proposed linear approximations. By comparing both figures it is clear that the non-linear system responses of Fig. 11 are adequately embodied by Fig. 7. This confirms that the use of the linear approximations for the study of perturbation rejection is appropriate and sufficient for this system.

Consider that the stator currents are perturbed by a colored noise comprised of white noise filtered by the weighting function $G_W(s) = 1/(s+1)$; thus the perturbations are mainly low frequency. Simulations with similar conditions to those of Figs. 9 and 10 were performed, but in this case the colored noise perturbation was

used in both stator currents at the same time. The resulting responses are shown in Fig. 12, which also provides the responses obtained with the standalone FOC controller (19) using the same perturbation signals. A first observation from this figure is that closing *either* the flux or torque control loops increases the perturbation rejection characteristics of *both* the flux and the torque; this confirms the analysis of the past sections. The results of Fig. 12 are also predicted by the perturbation rejection analysis developed in Section 5.1 (summarized in Fig. 7). In particular, for low frequency perturbations such as the ones used in these simulations, the overall perturbation rejection level for the flux is similar when closing either the flux or the torque control loop. In contrast, the overall perturbation rejection level for the torque is lower when operating the torque in closed loop. It can be concluded that closing the torque loop yields the best overall perturbation rejection for both the torque and the flux; this is confirmed by the responses of Fig. 12, which were obtained using the non-linear model.

6. Flux-torque cross-coupling case 2: perturbed rotor resistance

In this section the cross-coupling and perturbation rejection characteristics studied previously are extended to the perturbed FOC case. This will also reveal a caveat: it is not possible to use both a flux and a torque controller at the same time if there are perturbations in the slip angular velocity.

The main features of the cross-coupling characteristics of the flux-torque subsystem are contained in the MSF. In the last section it was found that when $\sigma_r = 1$ the MSF of this system is given by
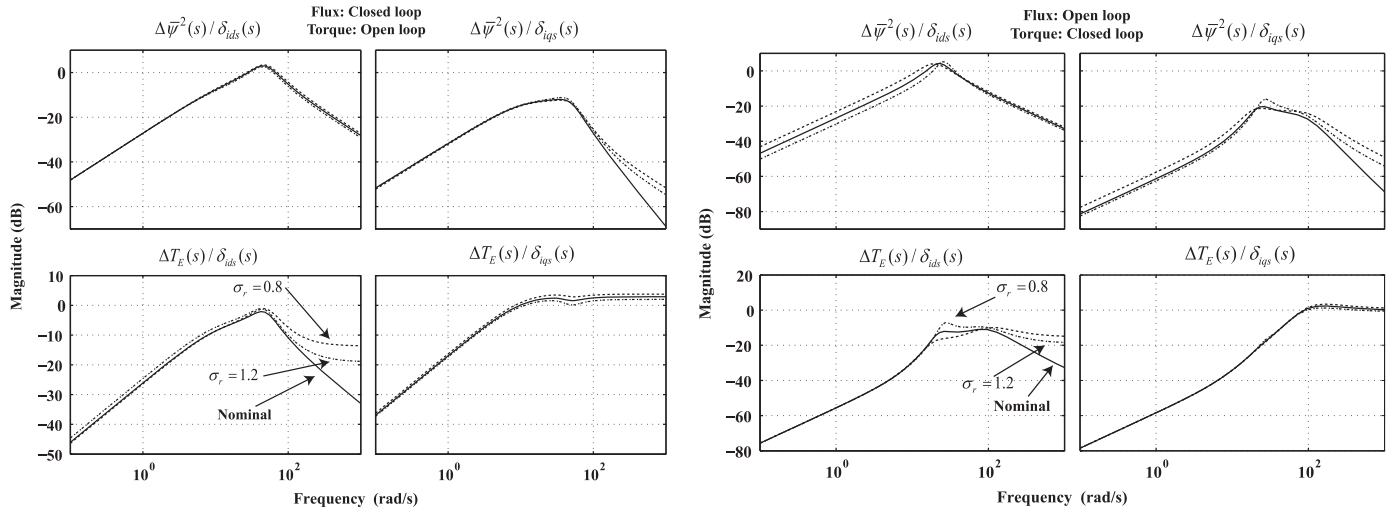
Fig. 14. Stator currents perturbations rejection perturbation characteristics of the flux-torque subsystem using external flux or torque controllers (31) and rotor resistance perturbations.
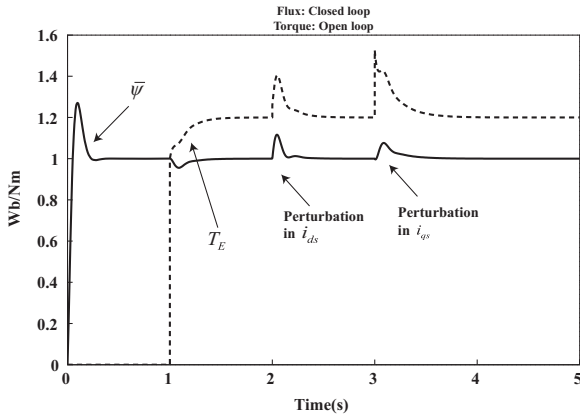

Fig. 15. Simulated flux and torque responses considering a rotor resistance perturbation of 20% and an external flux controller.
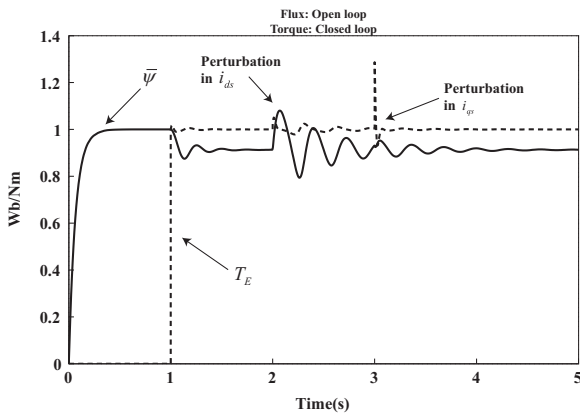

Fig. 16. Simulated flux and torque responses considering a rotor resistance perturbation of 20% and an external torque controller.

(26). In general, when $\sigma_r \neq 1$ the MSF of system (25) is:

$$\gamma(s) = \frac{g_{\psi q}(s)g_{Td}(s)}{g_{\psi d}(s)g_{Tq}(s)}$$

$$= \gamma(s) = \frac{k_1 s^3 + k_2 s^2 + k_3 s + 2a_1^5 a_2^2 \overline{\psi}_{r0}^8 K_T^4 \sigma_r T_{r0}^2 + 4a_1^3 a_2^4 \overline{\psi}_{r0}^4 K_T^2 \sigma_r^3 T_{r0}^4 + 2a_1 a_2^6 \sigma_r^5 T_{r0}^6}{k_4 s^3 + k_5 s^2 + k_6 s + 2a_1^5 a_2^2 \overline{\psi}_{r0}^8 K_T^4 \sigma_r T_{r0}^2 + 4a_1^3 a_2^4 \overline{\psi}_{r0}^4 K_T^2 \sigma_r^3 T_{r0}^4 + 2a_1 a_2^6 \sigma_r^5 T_{r0}^6}$$

(32)

Coefficients k_1-k_6 have been omitted due to lack of space.

It is common practice to evaluate the MSF through Nyquist plots when applying the ICAD framework [43]. The Nyquist plot of (32) using the motor parameters of Table 1 is shown in Fig. 13 for several values of σ_r. As it can be observed, this figure confirms that $\gamma(0) = 1$. This important observation indicates that all perturbation rejection characteristics found in the last section are preserved even if there are perturbations on the rotor resistance or the slip angular velocity.

Considering controllers (31), the resulting perturbation rejection characteristics of the flux-torque subsystem are summarized in Fig. 14 for several levels of rotor resistance perturbation. The only relevant difference between the perturbed and nominal cases is that the torque seems to be more sensible to δ_{ids} perturbations at higher frequencies. There are no additional significant differences in the perturbation rejection characteristics when the FOC controller is detuned.

6.1. Closed loop equilibrium point considerations

The introduction of external flux or torque control loops brings additional equilibrium point considerations. For instance, let a flux control loop as in Fig. 2 be used, so that the flux magnitude reaches the desired reference in steady state, i.e. $\overline{\psi}_0 = \overline{\psi}_r$. The required equilibrium current i_{ds0} so that $\overline{\psi}_0 = \overline{\psi}_r$ can be calculated by solving eq. (11) for i_{ds}. Substituting ϕ_0 and i_{qs0} (which are not modified by the external flux controller) from (19) yields:

$$i_{ds0} = \pm \frac{\sqrt{a_1 \overline{\psi}_{r0}^4 K_T^2 + a_2^2 T_{r0}^2 (\sigma_r^2 - 1)}}{K_T a_2 \overline{\psi}_{r0}}$$

(33)

If $\sigma_r = 1$ then i_{ds0} is equal to the nominal FOC input (19); however, when $\sigma_r \neq 1$ the external high-gain flux controller drives i_{ds} into (33). Accordingly, the generated steady state torque is also modified. By considering that the flux reaches the desired reference $\overline{\psi}_0 = \overline{\psi}_r$ and recalling Eq. (9), the generated torque now yields:

$$T_{E0} = \sigma_r T_{r0}$$

(34)

Eqs. (33)–(34) show that it is not possible to reach the desired steady state flux and torque *at the same time* by modifying the stator current i_{ds} in the presence of slip angular velocity perturbations. A similar conclusion can be obtained when the analysis is made using an external torque control loop. That is, if $\sigma_r \neq 1$ and the stator current i_{qs} is modified so that $T_{E0} = T_r$, then $\overline{\psi}_0 \neq \overline{\psi}_r$.

Simulations with the same conditions as those of Figs. 9 and 10 are carried out. However, in this case a rotor resistance

Current-Fed Non-linear model + perturbed FOC control + stator currents perturbations + external flux/torque controllers
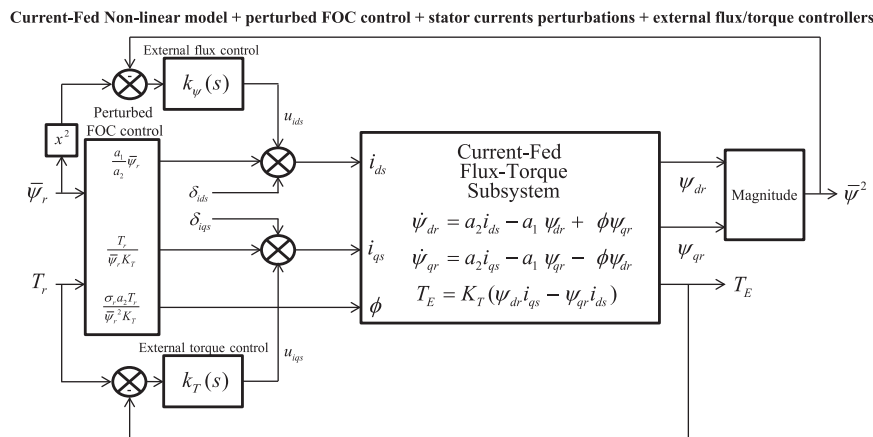

Fig. 17. Current-fed flux-torque subsystem with perturbed FOC control, stator currents perturbations and external flux and torque controllers
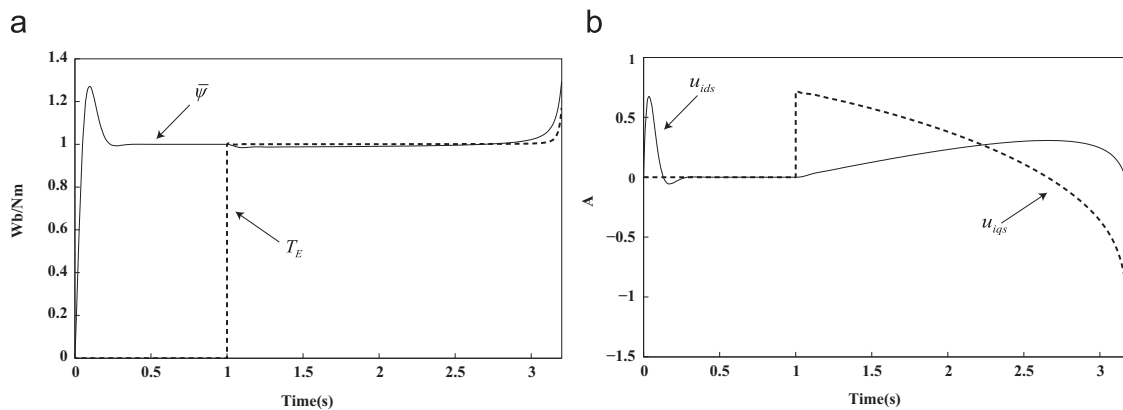

Fig. 18. Flux, torque and control effort responses when both channels are operated in closed loop.

perturbation modeled by $\sigma_r = 1.2$ is introduced, which modifies the nominal FOC input obtained with (19). Recall that the flux reference is fixed at 1 Wb, while the initial torque reference is equal to zero and changed to 1 Nm at $t=1$ s. In addition, recall that a perfectly tuned FOC controller would produce the desired torque change without affecting the flux.

Fig. 15 shows the flux and torque responses when the flux control loop is closed with a 20% of rotor resistance perturbation. The first observation is the well-known loss of flux-torque decoupling due to the FOC controller *detuning*. This is evident at $t=1$ s where the torque reference is changed from 0 to 1 Nm. When the flux control loop is closed the system converges to the equilibrium point as discussed in the last paragraphs, *i.e.* $\overline{\psi}_0 = \overline{\psi}_r$ and $T_{E0} = \sigma_r T_{r0}$. In addition, it is confirmed that the system is still able to reject both perturbations δ_{ids} and δ_{iqs}. Note that the torque *is rejecting the stator currents perturbations* (it returns to its "previous" level), but the equilibrium point has deviated from the desired steady state values due to the rotor resistance perturbations. In a similar manner Fig. 16 shows the case when the torque loop is closed. In this condition the flux equilibrium point deviates from the desired reference. Nonetheless, both flux and torque are able to reject the stator currents perturbations.

Figs. 15 and 16 confirm that the stator currents perturbation rejection properties of the flux-torque subsystem are maintained even in the presence of slip angular velocity deviations (in this case due to rotor resistance perturbation). However, undesirable equilibrium point deviations are also introduced. In this context one may ask: *is it possible to modify i_{ds} and i_{qs} independently so that both the flux and torque reach their desired references?* The equilibrium point analysis of Section 3 indicates, through Eq. (9), that it is possible for the machine to generate the desired flux and torque

Table 3
Effect of negative stator current levels.

Condition	$g_{\psi d}(s)$	$g_{Tq}(s)$
Nominal	$\dfrac{44.5(s+15.4)}{s^2+30.8s+493.4}$	$\dfrac{1.4(s^2+15.4s+511.8)}{s^2+30.8s+493.4}$
Negative i_{ds0}	$\dfrac{19.7(s-5.4)}{s^2+30.8s+493.4}$	$\dfrac{18.8(s+36.5)}{s^2+30.8s+493.4}$
Negative i_{qs0}	$\dfrac{0.61(s^2+36.3s+1155)}{s^2+30.8s+493.4}$	$\dfrac{0.58(s^2-5.7s-139.2)}{s^2+30.8s+493.4}$

levels in steady state *only when the slip angular velocity is properly driven*. This can be demonstrated in general by recalling Eq. (11), which represents the equilibrium value of i_{ds}, and solving i_{ds0} so that $\overline{\psi}_0^2 = \overline{\psi}_{r0}^2$:

$$i_{ds0} = \pm \sqrt{\frac{\overline{\psi}_{r0}^2 \left(a_1^2 + \phi_0^2\right)}{a_2^2} - i_{qs0}^2} \qquad (35)$$

On the other hand, substituting (6) into (8) yields:

$$T_{E0} = \frac{K_T \phi_0}{a_2}\left(\frac{i_{qs0}^2\left(a_2^2\phi_0^2 + a_1^2 a_2^2\right) + i_{ds0}^2\left(a_1^2 a_2^2 + a_2^2\phi_0^2\right)}{\left(a_1^2 + \phi_0^2\right)^2}\right) \qquad (36)$$

It is possible to reach the equilibrium point defined by $\overline{\psi}_0^2 = \overline{\psi}_{r0}^2$ and $T_{E0} = T_{r0}$ if a solution for Eqs. (35)–(36) exists so that $T_{E0} = T_{r0}$. This can be proved not to be the case by substituting (35) into (36),
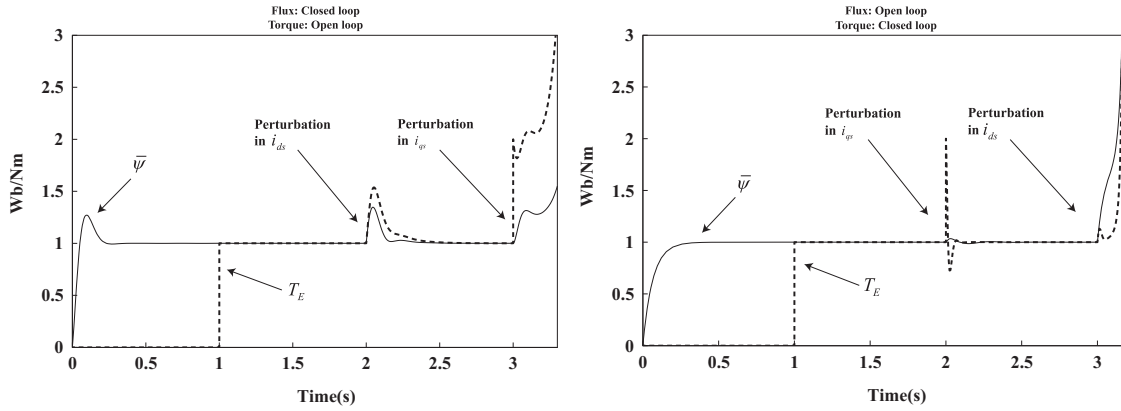
Fig. 19. Flux and torque responses for high level of stator currents perturbation.

which yields:

$$T_{E0} = \frac{K_T \phi_0}{a_2} \frac{\left(a_1^2 + \phi_0^2\right)\left(a_1^2 \overline{\psi}_r^2 + \phi_0^2 \overline{\psi}_r^2\right) + i_{qs0}{}^2 \left(a_1^2 a_2^2 + a_2^2 \phi_0^2 - a_1^2 a_2^2 - a_2^2 \phi_0^2\right)}{\left(a_1^2 + \phi_0^2\right)^2}$$

$$= \frac{K_T \phi_0}{a_2} \frac{\left(a_1^2 \overline{\psi}_r^2 + \phi_0^2 \overline{\psi}_r^2\right)}{\left(a_1^2 + \phi_0^2\right)} \qquad (37)$$

Eq. (37) indicates that if i_{ds0} is selected so that the desired equilibrium flux magnitude is reached, then *the generated torque does not depends on* i_{qs0}. Note that it is assumed that i_{ds0} exists -*i.e.* (35) is real. Substituting the perturbed slip angular velocity ϕ_0 from Eq. (19) into (37) yields:

$$T_{E0} = \sigma_r T_{r0} \qquad (38)$$

This indicates that for any i_{qs0} if a i_{ds0} exists such that $\overline{\psi}_0^2 = \overline{\psi}_{r0}^2$, then the equilibrium torque will always be $\sigma_r T_{r0}$. Note that the difference between eqs. (34) and (38) is that an arbitrary value for i_{qs0} was considered in (38); however, it is still assumed that i_{ds0} exists.

The fact that it is not possible to reach the equilibrium point $\overline{\psi}_0^2 = \overline{\psi}_{r0}^2$ and $T_{E0} = T_{r0}$ when $\sigma_r \neq 1$ is also contained in the dynamical cross-coupling analysis derived in Section 6 (using individual channels, Eqs. (27)–(28)). Recall that the individual channels represent the input-output relationship of the open loop variables when a closed loop controller is used in other channel. For instance, consider that the flux is operated in closed loop as in Fig. 2. It is necessary to determine if it is possible to control the torque by driving the input u_{iqs} (*i.e.* the external control input over stator current i_{qs}). In this case the ICAD analysis indicates that the system may be decomposed as shown in Fig. 3, with the difference that $u_{iqs} \neq 0$ is now allowed. The torque response due to any deviation of the stator current i_{qs} from the FOC nominal input (*i.e.* Δi_{qs}) is given by $g_{\psi d}(s)\left(1 - \gamma(s) h_T(s)\right)$, whose steady state gain was determined to be equal to zero. It is important to note that Δi_{qs} includes *both* the perturbations δ_{iqs} and the external control input u_{iqs}. Therefore, any modification in u_{iqs} yields the same result as a perturbation δ_{iqs}. This allows concluding that in steady state constant values for u_{iqs} are *rejected* in the same manner as constant δ_{iqs} perturbations. Hence, it is not possible to drive the torque by modifying i_{qs} at the same time as the flux is controlled via i_{ds} if the slip angular velocity is perturbed. A similar conclusion can be obtained for the case when the torque is operated in closed loop via i_{qs}; in this case it is not possible to drive the flux by modifying i_{ds}.

To illustrate the discussion of the last paragraph, Fig. 18a shows a digital simulation when both the flux and the torque control loops are operated at the same time using the control scheme of

Fig. 17 with 5% of rotor resistance perturbation (*i.e.* $\sigma_r = 1.05$). No additional stator current perturbations were included in order to isolate the equilibrium point problem. All other conditions are kept as in the simulation of Fig. 9. It can be observed that the flux and torque are maintained close to the desired references (1 Wb-1 Nm) until the system becomes unstable around 2.6 s. This behavior is better understood by looking at the control effort of the flux and torque controllers shown in Fig. 18b. It is clear that the controllers diverge due to the steady state gain of the individual channels, which is equal to zero. In particular, u_{ids} is constantly increasing to maintain the flux level while u_{iqs} is constantly decreasing to maintain the torque level.

Another observation regarding Fig. 18b is that the system becomes unstable once u_{iqs} reaches negative values. This is due to the torque being dependent on the flux magnitude, which is itself dependent on the magnitude of the stator currents due to the cross-coupling, *i.e.* $T_E \alpha \overline{\psi} \alpha \sqrt{i_{ds0}{}^2 + i_{qs0}{}^2}$. Once i_{qs} is negative any further decrement to this variable tends to *increase* the flux magnitude and therefore to increase the torque. This is equivalent to a sign change within the closed loop. Table 3 shows transfer functions $g_{\psi d}(s)$ and $g_{Tq}(s)$, the diagonal elements of (25), while considering nominal and negative values for i_{ds0} and i_{qs0}. Note that in fact i_{qs} can be negative in normal operation conditions if $T_r < 0$; however, in this case ϕ will also be negative and the sign change in $g_{Tq}(s)$ is avoided.

An additional characteristic of the equilibrium point can be observed. Consider that the flux channel is closed; then, by recalling Eq. (35) it is clear that it is possible for i_{ds0} to not exist if $|i_{qs0}|$ is sufficiently high. This condition can be brought by either an excessive δ_{iqs} perturbation or by a combination of a high load factor, defined as $L_F = \|T_r\|/\|\psi_r^2\|$, and rotor resistance perturbations $\sigma_r < 1$. The last condition can also be easily derived from (33). A similar conclusion is obtained when the torque channel is operated in closed loop. In this case the required steady state level of i_{qs} so that $T_{E0} = T_{r0}$ can be obtained by substituting $T_{E0} = T_{r0}$ in (36) and solving for i_{qs0}:

$$i_{qs0} = \sqrt{\frac{T_{r0} a_2 \left(a_1^2 + \phi_0^2\right)^2 - i_{ds0}^2 K_T \phi_0 \left(a_1^2 a_2^2 + a_2^2 \phi_0^2\right)}{\left(a_2^2 \phi_0^2 + a_1^2 a_2^2\right) K_T \phi_0}} \qquad (39)$$

Eq. (39) indicates that a high level of δ_{ids} perturbations, hence a greater i_{ds0}, will induce equilibrium point problems.

Fig. 19 shows the torque and flux responses when high level of perturbations are used (100% of the nominal current values). All other conditions are kept as in previous simulations. It is observed that a high level of perturbation can be rejected only when the corresponding loop is closed. For instance, when the flux channel

is closed a high level of δ_{ids} can be rejected while a high level of δ_{iqs} induces instability.

A summary of the observed phenomena on the equilibrium point is presented next:

1. The equilibrium point $\overline{\psi}_0 = \overline{\psi}_{r0}$ and $T_{E0} = T_{r0}$ exists **iff** $\sigma_r = 1$. Hence, if controllers with integral action are used for channels (22) simultaneously then the closed loop system will not converge when $\sigma_r \neq 1$. It can be concluded that any control scheme which intends to control the flux magnitude and torque levels simultaneously requires actively compensating the slip angular velocity.
2. Sufficiently negative values in i_{qs} or i_{ds} will induce a sign change within either the flux or torque channels; this normally leads to instability. Note that here i_{qs} is considered negative when $\text{sign}\{i_{qs}\} \neq \text{sign}\{\phi\}$.
3. While operating the flux channel in closed loop, the equilibrium point $\overline{\psi}_0 = \overline{\psi}_{r0}$ does not exist when δ_{iqs0} is high and/or when $\sigma_r < 1$ and the motor is operated with a high load factor.
4. While operating the torque channel in closed loop, the equilibrium point $T_{E0} = T_{r0}$ does not exist when δ_{ids0} is high.

Other equilibrium point problems have been identified for FOC controlled IMs in the past [16–19]; however, these reports did not deal with the multivariable aspect of the flux-torque subsystem.

7. Conclusions

The flux-torque subsystem of the FOC-controlled IM has been studied using the multivariable control system framework referred to as ICAD. In particular, the study focus is the cross-coupling of the flux-torque subsystem considering an IFOC flux-torque controller subject to stator currents and rotor resistance perturbations.

If stator currents are considered as inputs and the flux magnitude and torque as outputs, it has been shown that the system contains a transmission zero which introduces particular perturbation rejection characteristics. This allows for complete stator currents perturbation rejection in the steady state closing either the flux or the torque channels using external controllers. These steady state results have been extended dynamically using the MSF, a key component of ICAD. The analysis shows that closing only the torque channel with an external controller provides better performance and exploits the aforementioned perturbation rejection properties. The results also confirm that simultaneous control of the flux and torque is not possible in the presence of slip angular velocity perturbations. In particular, it has been shown that this is due to the same transmission zero, which provides the system with inherent stator currents perturbation rejection properties.

An analysis of the equilibrium point characteristics of FOC schemes has been also included in this article and the dynamical findings are in line with this analysis. A new set of characteristics which can lead to problems with the existence of an ideal equilibrium have been characterized. It has been observed that bifurcations may arise due to the non-existence of the desired equilibrium point when flux and torque are controlled simultaneously in the presence of slip angular velocity and stator currents perturbations. In particular, if the slip angular velocity is perturbed a combination of stator currents so that both flux magnitude and torque reach their desired reference does not exist. In these conditions a flux-torque controller could become unstable if, for instance, integral action is used. In addition, there are also equilibrium point existence problems in the presence of excessive stator current or slip angle perturbation that could induce instability in closed loop. Specifically, with slip angular velocity

perturbations the decoupling of the flux- and torque-producing currents is lost. In these circumstances a perturbation on the torque-producing current may cause a flux magnitude perturbation that cannot be rejected by the flux-producing current; instead instability can be induced.

While the work presented in this article is mainly theoretical, the characterization of the cross-coupling characteristics, the perturbation rejection properties, and the performance of the control system have been based on classical frequency analysis tools. Moreover, the main results for the evaluation of the perturbation rejection characteristics of the flux-torque subsystem have been elucidated through representative simulations. These examples show that the findings presented in this work can be easily incorporated into real-world applications.

References

[1] Chiasson J. Modelling and high-performance control of electric machines. USA: IEEE Press; 2005.
[2] Bin W. High power converters and AC drives. USA: IEEE Press; 2006.
[3] Rodríguez J, Kennel R, Espinoza J, Trincado M, Silva C, Rojas C. High-performance control strategies for electrical drives: an experimental assessment. IEEE Trans Ind Electron 2012;59(2):812–20.
[4] Basilio JC, Silva JA, Rolim LGB, Moreira MV H. design of rotor flux oriented current-controlled induction motor drives: speed control, noise attenuation and stability robustness. IET Control Theory Appl 2010;4(11):2491–505.
[5] Ebrahim OS, Salem MF, Jain PK, Badr MA. Application of linear quadratic regulator theory to the stator field-oriented control of induction motors. IET Electr Power Appl 2010;4(8):637–46.
[6] Hinkkanen M, Harnefors L, Luome J. Reduced-order flux observers with stator-resistance adaptation for speed-sensorless induction motor drives. IEEE Trans Power Electron 2010;25(5):155–62.
[7] Fnaiech MA, Khadraoui S, Nounou HN, Nounou MN, Guzinski J, Abu-Rub H, et al. A measurement-based approach for speed control of induction machines. IEEE J Emerg Sel Top Power Electron 2014;2(2):308–18.
[8] Uddin MN, Zhi-Rui H, Hossain AB. Development and implementation of a simplified self-tuned neuro–fuzzy-based IM drive. IEEE Trans Ind Appl 2014;50(1):51–9.
[9] Konstantopoulos GC, Alexandridis AT, Mitronikas ED. Bounded nonlinear stabilizing speed regulators for VSI-fed induction motors in field-oriented operation. IEEE Trans Control Syst Technol 2014;22(3):1112–21.
[10] Chang GW, Espinosa-Perez G, Mendes E, Ortega R. Tuning rules for the PI gains of field-oriented controllers of induction motors. IEEE Trans Ind Electron 2000;47(3):592–602.
[11] Lee J, Hong J, Nam K, Ortega R, Praly L, Astolfi A. Sensorless control of surface-mount permanent-magnet synchronous motors based on nonlinear observers. IEEE Trans Power Electron 2010;25(2):290–7.
[12] Yongjun Z, Chunhui H. Generalized predictive control with load torque observation for induction motor. In: Proceedings of the 30th Chinese control conference; 2011. p. 3467–71.
[13] Peng K, Zhao J. Speed control of induction motor using neural network sliding mode controller. In: Proceedings of the international conference on electric information and control engineering; 2011. p. 6125–6129.
[14] Khan MA, Uddin MN, Rahman MA. Real-time performance investigation of an intelligent controller based speed control of induction motor drives. In: Proceedings of the IEEE international conference on electrical machines and drives; 2011. p. 161–169.
[15] Kumar N, Chelliah T, Srivastava S. Adaptive control schemes for improving dynamic performance of efficiency-optimized induction motor drives. Corrected Proof, Available online 26March. ISA Trans 2015 10.1016/j.isatra.2015.02.011, in press.
[16] Bazanella AS, Reginattol R, Osvaldo AV. Robustness margins for indirect field-oriented control of induction motors. IEEE Trans Autom Control 2000;45(6):1226–31.

[17] Salas F., Reginatto R., Gordillo F., Aracil J. Bogdanov-takens bifurcation in indirect field oriented control of induction motor drives. In: Proceedings of the 43rd IEEE conference on decision and control; 2004. p. 4357–62.

[18] Reginatto R, Salas F, Gordillo F, Aracil J. Zero-Hopf bifurcation in indirect field oriented control of induction motors analysis and control of chaotic systems. In: Proceedings of the First IFAC conference on analysis and control of chaotic systems; 2006. p. 309–14.

[19] Gordillo F, Salas F, Ortega R, Aracil J. Robust tuning of the speed loop in indirect field oriented control of induction motors. Automatica 2002;38 (5):829–35.

[20] Khalil HK, Strangas EG, Jurkovic S. Speed observer and reduced nonlinear model for sensorless control of induction motors. IEEE Trans Control Syst Technol 2008;17(2):327–39.

[21] Boldea I, Nasar S. Electric drives. Second Edition. USA: CRC Press; 2006.

[22] Vas P. Sensorless Vector and Direct Torque Control. USA: Oxford University Press; 1998.

[23] Travieso-Torresa J, Duarte-Mermoud M. Two simple and novel SISO controllers for induction motors based on adaptive passivity. ISA Trans 2008;47(1):60–79.

[24] Travieso-Torresa J, Duarte-Mermoud M. Control of induction motors: an adaptive passivity MIMO perspective. Int J Adapt Control Signal Process 2003;17(4):313–32.

[25] Zheng Q, Chen Z, Gao Z. A practical approach to disturbance decoupling control. Control Eng Pract 2009;17(9):1016–25.

[26] Xue W, Huang Y. Generalized Predictive Control with Load Torque Observation for Induction Motor. In: Proceedings of the 30th Chinese control conference; 2011. p. 6362–7.

[27] Guo B, Zhao Z. On convergence of the nonlinear active disturbance rejection control for MIMO Systems. SIAM J Control Optim 2013;51(2):1727–57.

[28] Rafa S, Larabi A, Barazane L, Manceur M, Essounbouli N, Hamzaoui A. Implementation of a new fuzzy vector control of induction motor. ISA Trans 2014;53(3):744–54.

[29] Bristol E. On a new measure of interaction for multivariable process control. IEEE Trans Autom Control 1966;11(1):133–4.

[30] Skogestad S, Postlethwaite I. Multivariable feedback control. UK: John Wiley & Sons; 2005.

[31] Amezquita-Brooks L, Ugalde-Loo CE, Liceaga-Castro E, Liceaga-Castro J. The multivariable structure function as an extension of the RGA matrix: relationship and advantages. Cybern Phys 2013;2(2):53–62.

[32] Amezquita-Brooks L, Liceaga-Castro J, Liceaga-Castro E. Speed and position controllers using indirect field-oriented control: a classical approach. IEEE Trans Ind Electron 2014;61(4):1928–43.

[33] Holmes D, McGrath B, Parker S. Current regulation strategies for vector-controlled induction motor drives. IEEE Trans Ind Electron 2012;59 (10):3680–9.

[34] Bazanella AS, Reginatto R. Robust tuning of the speed loop in indirect field oriented control of induction motors. Automatica 2001;37(11):1811–8.

[35] O'Reilly J, Leithead WE. Multivariable control by individual channel design. Int J Control 1991;54(1):1–46.

[36] Robertson SS, O'Reilly J, Leithead WE. Nyquist/Bode design for multivariable systems with parametric uncertainty. 3/1–3/4. Softw Appl 1997.

[37] Ugalde-Loo CE, Acha E, Liceaga-Castro E. Fundamental analysis of the electro-mechanical oscillation damping control loop of the static VAr compensation using individual channel analysis and design. IEEE Trans Power Deliv 2010;25 (4):3053–69.

[38] Ugalde-Loo CE, Amezquita-Brooks L, Liceaga-Castro E, Liceaga-Castro J. Structural robustness assessment of electric machine applications using individual channel analysis and design. Cybern Phys 2013;2(2):108–18.

[39] Amezquita-Brooks L, Liceaga-Castro E, Liceaga-Castro J. The structural robustness of the induction motor stator currents subsystem. Asian J Control 2014;16 (6):1632–45.

[40] Amezquita-Brooks L, Liceaga-Castro E, Liceaga-Castro, Ugalde-Loo CE. Induction motor control: multivariable analysis and effective decentralized control of stator currents for high performance applications. IEEE Trans Ind Electron 2015, 10.1109/TIE.2015.2436360, in press.

[41] Doyle JC, Francis BA, Tannenbaum AR. Feedback control theory. USA: Macmillan Publishing; 1992.

[42] Amezquita-Brooks L, Liceaga-Castro J, Liceaga-Castro E. Induction motor identification for high performance control design. Int Rev Electr Eng 2009;4(5):1827–6660.

[43] Liceaga-Castro E, Liceaga-Castro J, Ugalde-Loo CE. Beyond the existence of diagonal controllers: from the relative array to the multivariable structure function. In: Proceedings of the IEEE conference on decision and control and european control conference; 2005. p. 7150–6, http://dx.doi.org/10.1109/CDC.2005.1583314.